

On the Interaction between Autonomous Mobility on Demand Systems and Power Distribution Networks — An Optimal Power Flow Approach

Alvaro Estandia, Maximilian Schiffer, Federico Rossi, Emre Can Kara, Ram Rajagopal, and Marco Pavone*

Abstract—In future transportation systems, the charging behavior of electric Autonomous Mobility on Demand (AMoD) fleets, i.e., fleets of self-driving cars that service on-demand trip requests, will likely challenge power distribution networks (PDNs), causing overloads or voltage drops. In this paper, we show that these challenges can be significantly attenuated if the PDNs’ operational constraints and exogenous loads (e.g., from homes or businesses) are considered when operating the electric AMoD fleet. We focus on a system-level perspective, assuming full cooperation between the AMoD and the PDN operators. Through this single entity perspective, we derive an upper bound on the benefits of coordination. We present an optimization-based modeling approach to jointly control an electric AMoD fleet and a series of PDNs, and analyze the benefit of coordination under load balancing constraints. For a case study in Orange County, CA, we show that coordinating the electric AMoD fleet and the PDNs helps to reduce 99% of overloads and 50% of voltage drops which the electric AMoD fleet causes without coordination. Our results show that coordinating electric AMoD and PDNs helps to level loads and can significantly postpone the point at which upgrading the network’s capacity to a larger scale becomes inevitable to preserve stability.

Index Terms—Electric Autonomous Mobility on Demand, Convex Optimization, Network Flow, Smart Grid, Unbalanced Optimal Power Flow

I. INTRODUCTION

FLEETS of autonomous electric vehicles servicing on-demand trip requests promise affordable urban mobility

A. Estandia is with Marain Inc., Palo Alto, CA 94306, USA. He worked on this paper while he was a visiting student at Stanford University. Email: alvaro@marain.com.

M. Schiffer is with the TUM School of Management, Technical University of Munich, Munich 80333, Germany. Email: schiffer@tum.de.

F. Rossi is with the NASA Jet Propulsion Laboratory, California Institute of Technology, Pasadena, CA 91109, USA. He worked on this paper while he was a Ph.D. student at Stanford University. Email: federico.rossi@jpl.nasa.gov.

E. C. Kara is with eIQ Mobility, San Jose, CA 95110, USA. He worked in this paper while he was with the Grid Integration Systems and Mobility Group, SLAC National Accelerator Laboratory, Menlo Park, CA 94025, USA. Email: eck@fastmail.com.

R. Rajagopal is with the Department of Civil and Environmental Engineering, Stanford University, Stanford, CA 94035, USA. Email: ramr@stanford.edu.

M. Pavone is with the Department of Aeronautics and Astronautics, Stanford University, Stanford, CA 94035, USA. Email: pavone@stanford.edu.

A. Estandia was supported by the Zeno Karl Schindler Foundation with a Master’s Thesis Grant. This research was supported by the National Science Foundation under the CAREER and CPS programs, and by the Toyota Research Institute (TRI). This article solely reflects the opinions and conclusions of its authors and not NSF, TRI or any other Toyota entity.

*Corresponding author

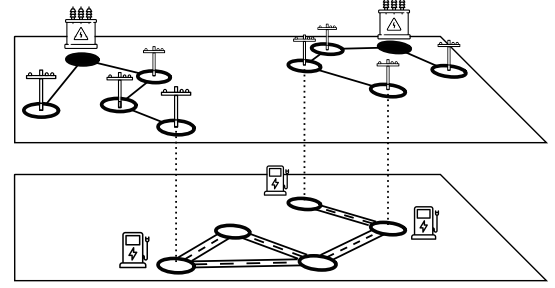


Fig. 1: Integration of a road network (bottom) and multiple power distribution networks (PDNs) (top). Typically, a road network spans across multiple PDNs and connects to the PDNs via charging station vertices. Besides charging stations that represent controllable loads, PDNs contain reference buses (typically substations) highlighted in black.

with reduced greenhouse gas emissions [1], decreased need for parking [2] and fewer road accidents [3]. Additionally, such a system offers further benefits from optimized central coordination, e.g., increased vehicle utilization compared to privately owned or decentrally controlled vehicles [2], and increased operational flexibility and efficiency compared to taxi, car-sharing, and ride hailing services. With these benefits, electric Autonomous Mobility on Demand (AMoD) service costs become competitive compared to private cars and public transit [4]. Furthermore, electric AMoD fosters the adoption of electric vehicles (EVs) as it allows an economically worthwhile operation through high utilization rates [1]. However, operating an electric AMoD fleet also bears inherent challenges as (re)charging vehicles adds a sizable load on the power distribution networks (PDNs). Studies on private EVs showed that uncoordinated charging can destabilize PDNs due to overloaded components or under-voltages [5]–[7]. Consequently, this would imply costly upgrades to the PDNs to secure stabilization. In contrast, we expect that intelligently coordinating the vehicles’ charging reduces such negative impacts and, thus, improves the utilization of the PDNs such that fewer power network upgrades are needed.

Controlling AMoD systems requires to solve a dispatching problem to assign vehicles to on-demand trip requests. The system’s performance increases if empty vehicles are proactively repositioned (rebalanced) in anticipation of future demand [8]. In the past decade, multiple approaches have been presented for the control of AMoD systems with

varying degrees of mathematical complexity. A first family of algorithms relies on heuristic rules for dispatching and rebalancing the fleet [9], [10]. More sophisticated methods use optimization instead of heuristics to control the AMoD system. Often, network flow models using fluidic relaxations, i.e., allowing for fractional vehicles and fractionally serviced trip requests are used [8]. Models of this type have been extended to consider road capacities and congestion [11], and to capture the interaction with public transit [12]. As network flow models do not capture the stochastic nature of a transportation problem, some studies focus on queueing-theoretical models [13] or Markov chains [14].

To control an *electric* AMoD system, an operator must keep track of a vehicle's state-of-charge (SoC) and recharge a vehicle's battery accordingly. Again, some heuristic approaches exist [15], [16]. Optimization-based approaches are so far not amenable to large-scale problems as they rely on mixed integer linear programs (MILPs) with discretized SoCs [17], [18]. Alternatively, queueing networks can be used to capture the stochastic nature of the electric AMoD problem [19].

The operation of an electric AMoD system induces a coupling between the power and the transportation systems. Thus, the electric AMoD fleet can be seen as a load that is controllable in time and space. Nonetheless, all previously mentioned studies neglect the impact of an electric AMoD system on the power grid although already a moderate amount of EVs may significantly increase electricity prices [20], and may negatively influence the power grid's reliability [21] and stability [22]. However, some approaches that account for a coupling between power networks and electric AMoD fleets exist. Some approaches consider the coupling implicitly via available capacities [23] or via prices [24] but control the electric AMoD fleet without considering its impacts on the power network explicitly. Only Rossi, Iglesias, Alizadeh, *et al.* [25] consider the impact of the fleet on the power network explicitly, introducing the Power in the Loop Autonomous Mobility on Demand (P-AMoD) model, a joint linear model that combines a network flow model for an electric AMoD system and a balanced single-phase DC model of a *transmission* network. However, this model does not consider PDNs yet. Further, a single-phase DC model is not sufficient to model a PDN as it assumes constant voltage magnitude, and neglects reactive power and link resistances [26]; instead, a three-phase model is necessary [27, Ch. 1]. So far, PDNs were only considered when determining optimal charging schedules for privately owned EVs which have to reach a certain SoC until the end of a given planning horizon [6], [7], [28]. Here, an instance of the Optimal Power Flow (OPF) problem can be solved, balancing necessary charging loads with PDN-specific constraints.

Concluding, individual aspects of our planning problem such as the control of an electric AMoD system or considering PDN models to optimally charge private EVs have been studied. However, to the best of our knowledge, no studies that tightly couple an electric AMoD system and PDN models to analyze their interdependencies exist so far.

With this work, our main goal is to address this gap. Specifically, the contribution of this paper is threefold: first,

we develop a mesoscopic model that captures the operations of and interaction between an electric AMoD system and a series of PDNs. Second, we embed this model in an optimization problem that yields an upper bound on the benefits of coordination between both systems. Third, we provide a case study in Orange County, CA where we study the impact of an electric AMoD system on the PDNs and evaluate the benefits of coordination.

The remainder of this paper is structured as follows: Section II presents a mesoscopic model for an electric AMoD system while Section III presents a model for a PDN. Section IV discusses the interaction between the electric AMoD system and a series of PDNs and introduces our approach for jointly optimizing both systems. Section V details our case study of Orange County, CA and presents results that allow analyzing the impact of electric AMoD systems on PDNs, highlighting the improvement potential of coordinating both systems. Section VI concludes this paper with a short summary of its main findings and an outlook on future research.

General Notation: Let \mathbb{R} denote the set of real and \mathbb{C} the set of complex numbers. We typeset vectors \mathbf{v} in bold lowercase, matrices \mathbf{Z} in bold uppercase, tuples \mathbf{v} in roman bold lowercase, and sets \mathcal{T} in calligraphic font. We use parentheses to build vectors $\mathbf{v} = (v_1 \ v_2)^T$, and brackets to denote concatenations or build block matrices, for example,

$$\mathbf{Z} = \begin{bmatrix} \mathbf{Z}_{11} & \mathbf{Z}_{12} \\ \mathbf{Z}_{12} & \mathbf{Z}_{22} \end{bmatrix}.$$

Further, $|\cdot|$ denotes the absolute value of a number or the cardinality of a set. For a matrix \mathbf{Z} , \mathbf{Z}^T is its transpose and \mathbf{Z}^H its conjugate transpose. The operator $\text{diag}(\mathbf{Z})$ on matrix \mathbf{Z} returns a vector with the matrix's diagonal entries. If acting on a vector, $\text{diag}(\mathbf{v})$ returns a diagonal matrix with \mathbf{v} in its diagonal. For a given complex power $s = p + jq$, $p \in \mathbb{R}$ is the active power, $q \in \mathbb{R}$ is the reactive power, and j is the imaginary unit. We denote a complex voltage $v \in \mathbb{C}$, by its magnitude $u = |v|$ and its angle $\theta = \arg(v)$.

II. MODELING ELECTRIC AMoD SYSTEMS

In an AMoD system, a fleet of autonomous vehicles services customer transport requests, i.e., picks up customers at their origin and brings them to their destination [2]. A fleet operator controls the AMoD fleet by assigning vehicles to customer requests and deciding on the route plan for each car. Besides origin-destination trips of customers, this route plan may comprise relocation trips in-between two customer trips as spatial and temporal mismatches between origins and destinations of different customer requests arise. In an electric AMoD problem, the fleet operator additionally decides on vehicle charging schedules as the fleet consists of EVs.

In this paper, we model an electric AMoD system through a linear network flow model as originally presented in [25] but reported here for completeness. To avoid integer variables, the model uses *i)* a fluidic vehicle approximation and *ii)* a road graph expanded along two dimensions: discrete time and vehicles' SoC. Additionally, we account for congestion using a threshold model.

a) *General road network representation:* We model the road network on a graph $G_R = (\mathcal{V}_R, \mathcal{A}_R)$ with a set of vertices $v \in \mathcal{V}_R$ and a set of road segment arcs $(v, w) \in \mathcal{A}_R$. We consider a set $\mathcal{T} = \{1, \dots, T\}$ of discrete equidistant time steps (each of duration $\Delta t \in \mathbb{R}^+$), and a set $\mathcal{C} = \{1, \dots, C\}$ of equidistant discrete battery charge levels (each of energy $E_c \in \mathbb{R}^+$).

While some vertices merely represent intersections or access points, others represent charging stations $\mathcal{S} \subseteq \mathcal{V}_R$ that allow recharging of vehicles. Each charging station $s \in \mathcal{S}$ has a charging rate $\delta_{C,s} \in \{1, \dots, C\}$ that denotes the amount of SoC that can be recharged in a single time step. Additionally, charging stations have a certain number of charging plugs $\tilde{S}_s \in \mathbb{R}^+$ that limit the number of concurrently charging vehicles.

Each arc $(v, w) \in \mathcal{A}_R$ is characterized by a distance $d_{v,w} \in \mathbb{R}^+$, a traversal time $t_{v,w} \in \{1, \dots, T\}$ and an energy consumption $c_{v,w} \in \{1, \dots, C\}$.

We model congestion using a threshold model, i.e., we assume that vehicles drive at the street's free-flow speed as long as their number is less than the street's capacity $f_{v,w} \in \mathbb{R}^+$.

b) *Expanded graph representation:* We use an expanded graph to model a vehicle's SoC over time. The expanded graph $G = (\mathcal{V}, \mathcal{A})$ is directed and has a vertex set $\mathcal{V} \subseteq \mathcal{V}_R \times \mathcal{T} \times \mathcal{C}$. Each vertex $\mathbf{v} \in \mathcal{V}$ is defined by a tuple $(v_{\mathbf{v}}, t_{\mathbf{v}}, c_{\mathbf{v}})$ that represents a vertex $v_{\mathbf{v}}$ of \mathcal{V}_R at a specific time $t_{\mathbf{v}}$ with a specific SoC $c_{\mathbf{v}}$. The resulting arc set \mathcal{A} consists of two subsets $\mathcal{A}_T \cup \mathcal{A}_S = \mathcal{A}$. An arc $(\mathbf{v}, \mathbf{w}) \in \mathcal{A}_T$ represents a spatial, time-dependent movement in the road network and must meet the following condition

$$\mathcal{A}_T = \{(\mathbf{v}, \mathbf{w}) \in \mathcal{A} \mid (v_{\mathbf{v}}, v_{\mathbf{w}}) \in \mathcal{A}_R, \\ t_{\mathbf{w}} - t_{\mathbf{v}} = t_{v_{\mathbf{v}}, v_{\mathbf{w}}}, c_{\mathbf{w}} - c_{\mathbf{v}} = c_{v_{\mathbf{v}}, v_{\mathbf{w}}}\},$$

i.e., i) $(v_{\mathbf{v}}, v_{\mathbf{w}})$ is a road arc, ii) its time expansion $t_{\mathbf{w}} - t_{\mathbf{v}}$ equals its traversal time $t_{v_{\mathbf{v}}, v_{\mathbf{w}}}$, and iii) its SoC expansion $c_{\mathbf{w}} - c_{\mathbf{v}}$ equals its consumption $c_{v_{\mathbf{v}}, v_{\mathbf{w}}}$. An arc $(\mathbf{v}, \mathbf{w}) \in \mathcal{A}_S$ represents a spatially static recharging process at a charging station and must meet the following condition

$$\mathcal{A}_S = \{(\mathbf{v}, \mathbf{w}) \in \mathcal{A} \mid v_{\mathbf{v}} = v_{\mathbf{w}} = s \in \mathcal{S}, \\ c_{\mathbf{w}} - c_{\mathbf{v}} = (t_{\mathbf{w}} - t_{\mathbf{v}})\delta_{C,s}\},$$

i.e., i) $v_{\mathbf{v}}$ and $v_{\mathbf{w}}$ are spatially equal and a charging station, and ii) the SoC difference $c_{\mathbf{w}} - c_{\mathbf{v}}$ equals the amount of energy recharged $(t_{\mathbf{w}} - t_{\mathbf{v}})\delta_{C,s}$.

c) *Electric AMoD model:* Besides this graph representation, we define a set of customer trip requests $\mathcal{M} = \{1, \dots, M\}$. Each trip $m \in \mathcal{M}$ is defined by a quadruple $(v_m, w_m, t_m, \lambda_m) \in \mathcal{V}_R \times \mathcal{V}_R \times \mathcal{T} \times \mathbb{R}^+$ that denotes its origin v_m , its destination w_m , its departure timestep t_m , and the customer rate λ_m . We assume a deterministic setting in which these requests are known or predicted for all timesteps. We introduce $f_0(\mathbf{v}, \mathbf{w}) : \mathcal{A} \rightarrow \mathbb{R}^+$ to represent the flow of rebalancing vehicles on arc (\mathbf{v}, \mathbf{w}) . Further, $N_I(\mathbf{v})$ denotes the number of vehicles available at vertex \mathbf{v} with charge level $c_{\mathbf{v}}$ at $t_{\mathbf{v}} = 1$. Analogously, $N_F(\mathbf{v})$ denotes the number of vehicles that must be at node $v_{\mathbf{v}}$ with charge level $c_{\mathbf{v}}$ at $t_{\mathbf{v}} = T$ and is zero for all other timesteps.

With this notation, a multi-commodity flow representation of the electric AMoD model holds as follows:

$$\sum_{\mathbf{u}: (\mathbf{u}, \mathbf{v}) \in \mathcal{A}} f_0(\mathbf{u}, \mathbf{v}) + \sum_{m=1}^M \mathbb{1}_{v_{\mathbf{v}}=w_m} \lambda_m^{t_{\mathbf{v}}, c_{\mathbf{v}}, \text{out}} + N_I(\mathbf{v}) \\ = \sum_{\mathbf{w}: (\mathbf{v}, \mathbf{w}) \in \mathcal{A}} f_0(\mathbf{v}, \mathbf{w}) + \sum_{m=1}^M \mathbb{1}_{v_{\mathbf{v}}=v_m} \mathbb{1}_{t_{\mathbf{v}}=t_m} \lambda_m^{c_{\mathbf{v}}, \text{in}} + N_F(\mathbf{v}) \quad \forall \mathbf{v} \in \mathcal{V} \quad (1)$$

$$\sum_{c=1}^C \lambda_m^{c, \text{in}} = \lambda_m \quad \forall m \in \mathcal{M} \quad (2)$$

$$\sum_{t=1}^T \sum_{c=1}^C \lambda_m^{t, c, \text{out}} = \lambda_m \quad \forall m \in \mathcal{M} \quad (3)$$

Here, $\lambda_m^{c, \text{in}}$ is the rate of vehicles with charge c departing to service customer trip request m , $\lambda_m^{t, c, \text{out}}$ is the rate of vehicles with charge c arriving at time t after servicing customer trip request m , and $\mathbb{1}_x$ is the indicator function. Equation (1) secures flow conservation for rebalancing vehicles, ensures a sufficient number of empty vehicles in each vertex to cover originating trip requests, and enforces initial and final conditions on the vehicle location through N_I and N_F . Equation (2) distributes a given trip request to vehicles with different SoC. Analogously, Eq. (3) accumulates vehicles arriving at different times with different SoC.

d) *Precomputed customer routes:* To reduce the number of variables, we use precomputed vehicle routes, following the shortest-time path $r_{v \rightarrow w}$, for customer-carrying vehicles. Note that our threshold congestion model allows computing these shortest-time paths during preprocessing. Each path has a traveling time $t_{v \rightarrow w}$ and charge requirement $c_{v \rightarrow w}$. Thus, we have that

$$\lambda_m^{t, c, \text{out}} = \begin{cases} \lambda_m^{c + c_{v_m \rightarrow w_m}, \text{in}} & \text{if } t_m = t - t_{v_m \rightarrow w_m} \\ 0 & \text{otherwise} \end{cases} \quad \forall t \in \mathcal{T}, c \in \mathcal{C}, \forall m \in \mathcal{M}. \quad (4)$$

e) *Electric AMoD problem:* We now extend the basic constraints of the electric AMoD model to a complete electric AMoD problem. Specifically, we optimize the vehicles' rebalancing routes and charging schedules in order to minimize the

cost of operating the electric AMoD system:

$$\begin{aligned} & \underset{\substack{f_0, [\lambda_m^{c, \text{in}}]_{c \in \mathcal{C}}, \\ [\lambda_m^{t, c, \text{out}}]_{c \in \mathcal{C}, t \in \mathcal{T}, N_I, N_F}}}{\text{minimize}} & V_D \sum_{(\mathbf{v}, \mathbf{w}) \in \mathcal{A}} d_{v_{\mathbf{v}}, v_{\mathbf{w}}} f_0(\mathbf{v}, \mathbf{w}) \\ & + \sum_{\substack{(\mathbf{v}, \mathbf{w}) \in \mathcal{A}_S: \\ v_{\mathbf{v}} = v_{\mathbf{w}} = s}} V_{\text{el}, s} [t_{\mathbf{v}}] \delta c_s f_0(\mathbf{v}, \mathbf{w}) \end{aligned} \quad (5a)$$

subject to

Eqs. (1) to (4) Electric AMoD model

$$\sum_{c_{\mathbf{v}}=1}^C f_0(\mathbf{v}, \mathbf{w}) \leq \bar{f}_{(v_{\mathbf{v}}, v_{\mathbf{w}}), t_{\mathbf{v}}} \quad \forall (v_{\mathbf{v}}, v_{\mathbf{w}}) \in \mathcal{A}_R, t_{\mathbf{v}} \in \mathcal{T} \quad (5b)$$

$$\sum_{\substack{(\mathbf{v}, \mathbf{w}) \in \mathcal{A}_S: \\ v_{\mathbf{v}} = v_{\mathbf{w}} = s}} f_0(\mathbf{v}, \mathbf{w}) \leq \bar{S}_s \quad \forall s \in \mathcal{S}, t \in \mathcal{T} \quad (5c)$$

$$g_I(N_I) = 0 \quad (5d)$$

$$g_F(N_F) = 0 \quad (5e)$$

The objective function Eq. (5a) minimizes the operational cost of the electric AMoD system, considering distance costs $V_D \in \mathbb{R}$ for rebalancing vehicles and time-varying electricity costs $V_{\text{el}, s} \in \mathbb{R}$ for recharging vehicles at a charging station $s \in \mathcal{S}$. Equations (1) to (4) impose general flow conservation while Eq. (5b) applies the threshold congestion model to rebalancing flows. As customer-carrying flows are fixed, we do not consider these directly in Eq. (5b). Instead, we adjust $\bar{f}_{(v_{\mathbf{v}}, v_{\mathbf{w}}), t_{\mathbf{v}}}$ by subtracting the customer carrying flow on each road arc from its maximum capacity for each time step $t_{\mathbf{v}} \in \mathcal{T}$. It may happen that the pre-routed vehicles congest a road link. In this case, we set the residual capacity $\bar{f}_{(v_{\mathbf{v}}, v_{\mathbf{w}}), t_{\mathbf{v}}}$ for that link to zero. Equation (5c) limits the number of vehicles that can use a charging station concurrently according to the number of charging plugs at each station. We impose initial and final conditions on vehicles by Eqs. (5d) and (5e).

The electric AMoD problem Eq. (5) has $TC(|\mathcal{A}_R| + |\mathcal{S}|) + CM + TC|\mathcal{V}_R| + C|\mathcal{V}_R|$ decision variables. Here, the dominant term CM admits an upper bound $\mathcal{O}(TC|\mathcal{V}_R|^2)$.

A few comments are in order. First, we consider discrete time steps as well as discrete SoC levels. From a mesoscopic viewpoint, these discretizations bear sufficient accuracy while improving the model's computational tractability significantly. Second, the network flow model treats vehicles and customers as fractional flows; accordingly, it is not suitable for real-time control of electric AMoD fleets. Again, this accuracy loss is acceptable at a mesoscopic level and does not restrict our scope to determine an *upper bound* on the achievable performance of coordination between electric AMoD and PDN operators. Note that our solution can still be used as a reference for a lower-level microscopic controller [cf. 29]. Third, we limit the vehicle flow on a given road link to its capacity and assume vehicles to travel at free flow speed accordingly. Such a threshold congestion model is in line with the accuracy requirements of our mesoscopic viewpoint. If necessary, more sophisticated congestion models can easily be integrated into our modeling approach but worsen the computational tractability. Fourth, we assume that future trip requests are known or estimated with

a high degree of accuracy. While the development of tools to estimate AMoD demand is beyond the scope of this paper, remarkably accurate algorithms are available in the literature to predict future trip requests in AMoD systems [e.g., 30]. Fifth, we optimize only rebalancing trips and fix customer trips to their shortest-time-paths. In principle, including the optimization of customer-carrying trips could yield solutions with lower cost; however, our prior work [25] has shown that the inclusion of customer-carrying trips in the optimization problem results in a small decrease in cost at the price of a huge increase in computational complexity. Further, note that although the route of customer-carrying trips is fixed, the SoC of customer-carrying vehicles is part of the optimization problem. Finally, the electric AMoD problem Eq. (5) may become infeasible if the number or the distribution of customer trip requests exceeds the customer-carrying capacity of the electric AMoD system. Here, we assume that the problem is always feasible as the fleet operator can reject or postpone trip requests to ensure feasibility. This is in line with common practice in today's taxi or ride hailing platforms. Nonetheless, a mechanism to decide which trips should be rejected or postponed exceeds the scope of this paper.

III. MODELING UNBALANCED POWER DISTRIBUTION NETWORKS

This section provides the basics of modeling unbalanced PDNs which we use to integrate the PDNs into an electric AMoD model. First, we introduce an unbalanced PDN model in Section III-A. Then, we define the optimal power flow problem in Section III-B.

A. Unbalanced power distribution network model

In the following, we consider only radial network structures which is the typical configuration for PDNs [27, Ch. 1.1] and base our notation on [26]. Figure 2 shows an example of a radial PDN modeled as a directed graph $P = (\mathcal{N}, \mathcal{E})$ with a tree topology, consisting of a set of buses $\mathcal{N} = \{0, \dots, N\}$ and a set of links $\mathcal{E} \subset \mathcal{N}^2$. Each PDN has a reference bus which typically denotes a substation that connects the PDN to the transmission network (in Fig. 2 we highlight the reference bus 0 in black). The set $\mathcal{N}^+ = \mathcal{N} \setminus 0$ is the set of buses excluding the reference bus. Buses are connected by links (e.g., power lines, transformers, regulators), such that $(n, o) \in \mathcal{E}$ represents a link in P between n and o for which n lies in the

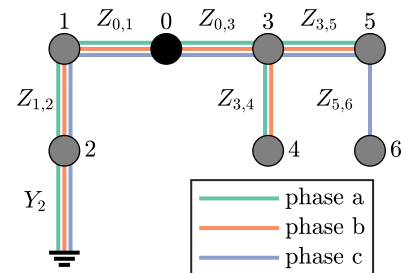


Fig. 2: Simple unbalanced distribution network with a tree topology.

single path between the reference bus 0 and bus o . As can be seen in Fig. 2, we model three phases by $\Phi = \{a, b, c\}$. We describe the set of phases in link $(n, o) \in \mathcal{E}$ by $\Phi_{n,o} \subseteq \Phi$ (e.g., $\Phi_{5,6} = \{c\}$). This leads to the set of phases in bus $n \in \mathcal{N}$ which includes the phases of all links connected to the bus (e.g., $\Phi_4 = \{b, c\}$), namely

$$\Phi_n = \left(\bigcup_{(m,n) \in \mathcal{E}} \Phi_{m,n} \right) \cup \left(\bigcup_{(n,o) \in \mathcal{E}} \Phi_{n,o} \right) \quad \forall n \in \mathcal{N}.$$

Each bus n has a time-invariant shunt admittance matrix $\mathbf{Y}_n \in \mathbb{C}^{|\Phi_n| \times |\Phi_n|}$, representing the admittance between the bus and ground. Further, each link (n, o) has a time-invariant impedance matrix $\mathbf{Z}_{n,o} \in \mathbb{C}^{|\Phi_{n,o}| \times |\Phi_{n,o}|}$.

We consider a discrete time model that tracks a series of steady states in the power network and neglects dynamic effects. This is appropriate if the discretization time is substantially longer than arising dynamic effects (i.e., in the order of minutes).

We consider a timespan $\mathcal{T} = \{1, \dots, T\}$ with time steps $t \in \mathcal{T}$, each having a length $\Delta t \in \mathbb{R}^+$. Each bus n has a time-dependent complex voltage $v_n^\phi[t] \in \mathbb{C}$ and a complex power injection $s_{\text{inj},n}^\phi[t] \in \mathbb{C}$ for each of its phases. Concurrently, each link shows a time-dependent current for each of its phases $i_{n,o}^\phi[t] \in \mathbb{C}$. For brevity, we use vectors for per-phase quantities: $\mathbf{v}_n = [v_n^\phi]_{\phi \in \Phi_n}$, $\mathbf{s}_{\text{inj},n} = [s_{\text{inj},n}^\phi]_{\phi \in \Phi_n}$, and $\mathbf{i}_{n,o} = [i_{n,o}^\phi]_{\phi \in \Phi_{n,o}}$. Herein, superscripts represent the projection onto specific phases. In Fig. 2, this projection holds as follows: consider $\mathbf{v}_4 = (v_4^b \ v_4^c)^T$ with $\Phi_4 = \{b, c\}$. Then, $\mathbf{v}_4^a = \mathbf{v}_4^a$. By convention, if the projection includes phases that are not present in the bus or the link, missing phases are set to zero. Hence, $\mathbf{v}_4^{abc} = (0 \ v_4^b \ v_4^c)^T$, since $a \notin \Phi_4$.

The current on each link obeys Ohm's law:

$$i_{n,o}^\phi[t] = \mathbf{Y}_{n,o}((\mathbf{v}_n[t])^{\Phi_{n,o}} - (\mathbf{v}_o[t])^{\Phi_{n,o}}) \quad (n, o) \in \mathcal{E}, t \in \mathcal{T},$$

with $\mathbf{Y}_{n,o} = \mathbf{Z}_{n,o}^{-1}$ [26].

Each bus is specified, either by its voltage or by its power injection such that the remaining quantity is a dependent variable [31, Ch. 6.4]. We refer to specified variables as *direct variables* and those that are dependent as *indirect variables*.

The reference bus specifies the reference voltage $v_{\text{ref}}^\phi[t] \in \mathbb{R}$ for the network:

$$v_0^\phi[t] = v_{\text{ref}}^\phi[t] \quad \phi \in \Phi_0, t \in \mathcal{T}. \quad (6)$$

Accordingly, the complex voltage \mathbf{v}_0 is the direct variable and the complex power injection $\mathbf{s}_{\text{inj},0}$ remains dependent.

For all other buses $n \in \mathcal{N}^+$, the complex power injection $\mathbf{s}_{\text{inj},n}$ is the direct variable, whereas the complex voltage \mathbf{v}_n remains dependent. These buses are called PQ buses since the active (p) and reactive power injection (q) are the direct variables. Herein, each PQ-bus has a time-varying uncontrollable load with complex power $\mathbf{s}_{\text{unc},n}[t] \in \mathbb{C}^{|\Phi_n|}$. These loads represent electricity demand from residential and commercial customers. We consider uncontrollable loads to be exogenous but known in advance within \mathcal{T} .

Controllable loads $\ell \in \mathcal{L} = \{1, \dots, L\}$ are defined by a tuple $(s_{\text{con},\ell}[t], n_\ell) \in \mathbb{C}^{|\Phi_{n_\ell}|} \times \mathcal{N}$ denoting their complex

power $s_{\text{con},\ell}$ and reference bus n_ℓ . These loads represent dispatchable generators or loads that can be throttled. With this notation, the power injections at PQ-buses are

$$\mathbf{s}_{\text{inj},n}[t] = -\mathbf{s}_{\text{unc},n}[t] - \sum_{\ell=1}^L \mathbb{1}_{n=n_\ell} \mathbf{s}_{\text{con},\ell}[t] \quad n \in \mathcal{N}^+, t \in \mathcal{T}. \quad (7)$$

Note that we model generators as negative loads without loss of generality. Further, we consider only wye-connected constant power loads which may require performing delta-to-wye conversions for some loads and approximating constant current and constant impedance loads as constant power ones. This simplification is commonly done in optimization frameworks [32].

Dependent variables result from the network topology and its controllable and uncontrollable loads. Specifically, they are related by the power flow equation [33]

$$\begin{aligned} \mathbf{s}_{\text{inj},n}[t] &= \text{diag}(\mathbf{v}_n[t] \mathbf{v}_n[t]^H \mathbf{Y}_n^H) \\ &+ \sum_{n:(n,o) \in \mathcal{E}} \text{diag}(\mathbf{v}_n^{\Phi_{n,o}}[t] (\mathbf{v}_n^{\Phi_{n,o}}[t] - \mathbf{v}_o^{\Phi_{n,o}}[t])^H \mathbf{Y}_{n,o}^H)^{\Phi_n} \end{aligned} \quad (8)$$

$t \in \mathcal{T}.$

Collectively, these equations allow us to model a radial time-invariant unbalanced PDN with time-varying controllable and uncontrollable loads.

A few comments are in order. First, we consider a discrete time model that tracks a series of steady states in the power network. As we are not interested in dynamic effects, model validity is preserved and the level of aggregation is aligned with our mesoscopic transportation model. Second, we consider a time-invariant PDN which cannot model control elements, e.g., step voltage regulators. Optimization frameworks commonly neglect these elements as they influence network characteristics only dependent on the slow dynamics of exogenous loads (see [28], [34]). Third, we assume that high-quality estimates of uncontrollable electrical loads are available. While deriving such estimates exceeds our scope, techniques to accurately estimate future power demand exist [e.g., 35].

B. Optimal Power Flow problem

The Optimal Power Flow (OPF) problem Eq. (9) optimizes a power network's state subject to its operational constraints and is often used for various tasks, e.g., operational or strategic planning, and pricing [36]. Here, we use an OPF problem for operational planning and decide on the controllable loads while optimizing a generic objective function $f(\cdot)$ subject to the power flow equation Eq. (8) and additional operational

constraints:

$$\begin{aligned} & \underset{[\mathbf{v}_n]_{n \in \mathcal{N}}, \mathbf{s}_0, [\mathbf{s}_{\text{con}, \ell}]_{\ell \in \mathcal{L}}}{\text{minimize}} && f(\cdot) \\ & \text{subject to} \end{aligned}$$

$$\text{Eq. (6)} \quad \text{Voltage at reference bus}$$

$$\text{Eq. (7)} \quad \text{Power injections}$$

$$\text{Eq. (8)} \quad \text{Power flow equation}$$

$$|v_n^\phi[t]| \geq u_{\min, n}^\phi \quad \phi \in \Phi_n, n \in \mathcal{N}^+, t \in \mathcal{T} \quad (9a)$$

$$|v_n^\phi[t]| \leq u_{\max, n}^\phi \quad \phi \in \Phi_n, n \in \mathcal{N}^+, t \in \mathcal{T} \quad (9b)$$

$$\left| \sum_{\phi \in \Phi} s_0^\phi[t] \right| \leq \hat{s}_0 \quad t \in \mathcal{T} \quad (9c)$$

$$p_{\text{con}, \ell}^\phi[t] \geq p_{\text{con}, \min, \ell}^\phi \quad \phi \in \Phi_{n_\ell}, \ell \in \mathcal{L}, t \in \mathcal{T} \quad (9d)$$

$$p_{\text{con}, \ell}^\phi[t] \leq p_{\text{con}, \max, \ell}^\phi \quad \phi \in \Phi_{n_\ell}, \ell \in \mathcal{L}, t \in \mathcal{T} \quad (9e)$$

$$q_{\text{con}, \ell}^\phi[t] \geq q_{\text{con}, \min, \ell}^\phi \quad \phi \in \Phi_{n_\ell}, \ell \in \mathcal{L}, t \in \mathcal{T} \quad (9f)$$

$$q_{\text{con}, \ell}^\phi[t] \leq q_{\text{con}, \max, \ell}^\phi \quad \phi \in \Phi_{n_\ell}, \ell \in \mathcal{L}, t \in \mathcal{T} \quad (9g)$$

Equations (6) to (8) denote the general power network model. Equations (9a) and (9b) constrain the voltage magnitude $|v_n^\phi[t]|$ to be within a minimal $u_{\min, n}^\phi \in \mathbb{R}$ and a maximal $u_{\max, n}^\phi \in \mathbb{R}$ value, according to regulations (e.g., ANSI C84.1) that require voltage to be kept within a given percentage of a nominal value. Equation (9c) limits the apparent power injected to the reference bus, i.e., conserves the rating of the substation transformer $\hat{s}_0 \in \mathbb{R}^+$. Equations (9d) to (9g) model the characteristics of controllable loads through lower and upper bounds on active power ($p_{\text{con}, \min, \ell}^\phi, p_{\text{con}, \max, \ell}^\phi \in \mathbb{R}$), and reactive power ($q_{\text{con}, \min, \ell}^\phi, q_{\text{con}, \max, \ell}^\phi \in \mathbb{R}$).

This OPF problem is non-convex because of the power flow equation Eq. (8) and lower bound constraints on voltage magnitudes Eq. (9a). Even the optimization of a balanced single-phase approximation of this problem remains an NP-hard problem [37].

a) Convex power flow surrogates: To combine the electric AMoD problem Eq. (5) and the OPF problem Eq. (9), we require the joint problem to be convex and, ideally, linear to preserve its computational tractability. Hence, we convexify the OPF problem using a power flow surrogate.

A power flow surrogate approximates the power flow equation Eq. (8) such that a convex, computationally tractable problem reformulation remains. Using such a power flow surrogate, we lose exact knowledge of the indirect variables which are approximated in the surrogate to preserve convexity.

Given the high relevance of the OPF problem, ample literature on power flow surrogates [36], [38] exists. However, most of these surrogates, as well as comparative studies, consider only balanced single-phase models as typically used in transmission networks [39].

For unbalanced three-phase models, only few power flow surrogates exist, and, to the best of our knowledge, no survey or benchmark classifies the suitability of these surrogates for specific problem structures. To close this gap, we analyzed three promising surrogates in a separate study [40]. For the sake of completeness, we briefly summarize these findings in

the following.

In our study, we compared a convex, semi-definite program (SDP) surrogate, the branch flow model SDP (BFM-SDP) [26], against two linear problem formulations, the branch flow model LP (BFM-LP) [26], [41] and the linearized power flow manifold LP (LPFM-LP) [42]. We used the charger maximization problem, which maximizes the power delivered to a series of charging stations across a distribution network as a benchmark because it challenges the power flow surrogates by pushing the network's state to the limits of its operational constraints.

We analyzed each surrogate evaluating its accuracy in approximating indirect variables for voltage magnitude Eqs. (9a) and (9b) and substation transformer rating Eq. (9c) constraints. Additionally, we analyzed the resulting constraint violations and computational times. In a nutshell, BFM-SDP yielded exact solutions on small instances but performed significantly worse than the other two approaches for both solution quality and computational time on large instances. LPFM-LP and BFM-LP revealed a trade-off between solution quality and computational time. While LPFM-LP yielded a better solution quality, e.g., 91.0 percent reduction on the mean average error in approximating bus voltage magnitudes, BFM-LP yielded 97.3 percent shorter computational times. Neither of these two surrogates violated the substation rating constraint.

Based on these results, we use the BFM-LP in this work as it preserves linearity in the joint problem while yielding sufficient solution quality and short computational times for our mesoscopic study. In the following, we briefly summarize this surrogate; we refer the reader to the original papers [26], [41] for elaborate explanations and to Estandia [40] for comparative studies.

b) Branch flow model linearization: We derive the branch flow model linearization by assuming fixed link losses and voltage ratios between phases in a bus [26], [41]: let $\tilde{\mathbf{i}}_{n,o} \in \mathbb{C}^{|\Phi_{n,o}|}$ be the fixed link current in link $(n,o) \in \mathcal{E}$ used to determine the fixed link losses. Let $\tilde{\mathbf{v}}_n \in \mathbb{C}^{|\Phi_n|}$ be the voltage used to determine the fixed voltage ratios in bus $n \in \mathcal{N}^+$. Then $\mathbf{\Gamma}_{n,o} \in \mathbb{C}^{|\Phi_{n,o}| \times |\Phi_{n,o}|}$, the matrix of fixed voltage ratios for link $(n,o) \in \mathcal{E}$, has entries

$$(\mathbf{\Gamma}_{n,o}[t])_{ij} = \frac{((\tilde{\mathbf{v}}_n[t])^{\Phi_{n,o}})_i}{((\tilde{\mathbf{v}}_n[t])^{\Phi_{n,o}})_j} \quad i, j \in \{1, \dots, |\Phi_{n,o}|\}, \\ (n,o) \in \mathcal{E}, t \in \mathcal{T}.$$

We define the following matrices to ease the notation:

$$\begin{aligned} \mathbf{W}_n[t] &= \mathbf{v}_n[t] \mathbf{v}_n[t]^H, \\ \mathbf{\Lambda}_{n,o}[t] &= \text{diag}((\mathbf{v}_n[t])^{\Phi_{n,o}} \mathbf{i}_{n,o}[t]^H), \\ \tilde{\mathbf{L}}_{n,o}[t] &= \tilde{\mathbf{i}}_{n,o}[t]^H \tilde{\mathbf{i}}_{n,o}[t] \quad (n,o) \in \mathcal{E}, t \in \mathcal{T}. \end{aligned}$$

With this notation, fixed link losses and voltage ratios, the power flow equation Eq. (8) admits a linear approximation

[33]:

$$\begin{aligned} & \sum_{m:(m,n) \in \mathcal{E}} \Lambda_{n,o}[t] - \text{diag}(\mathbf{Z}_{m,n} \tilde{\mathbf{L}}_{n,o}[t]) - \text{diag}(\mathbf{W}_n[t] \mathbf{Y}_n^H) \\ & + \mathbf{s}_{\text{inj},n}[t] = \sum_{o:(n,o) \in \mathcal{E}} (\Lambda_{n,o}[t])^{\Phi_n} \quad n \in \mathcal{N}, t \in \mathcal{T}, \end{aligned} \quad (10)$$

$$\begin{aligned} \mathbf{W}_o[t] = & (\mathbf{W}_n[t])^{\Phi_{n,o}} - (\mathbf{\Gamma}_{n,o}[t] \text{diag}(\Lambda_{n,o}) \mathbf{Z}_{n,o}^H \\ & + \mathbf{Z}_{n,o} (\mathbf{\Gamma}_{n,o}[t] \text{diag}(\Lambda_{n,o}))^H + \mathbf{Z}_{n,o} \tilde{\mathbf{L}}_{n,o}[t] \mathbf{Z}_{n,o}^H \\ & (n, o) \in \mathcal{E}, t \in \mathcal{T} \end{aligned} \quad (11)$$

Then, replacing Eq. (8) by Eqs. (10) and (11) in Eq. (9) yields the BFM-LP:

$$\begin{aligned} & \underset{\substack{[\mathbf{W}_n]_{n \in \mathcal{N}}, \\ [\Lambda_{n,o}]_{(n,o) \in \mathcal{E}}, \\ \mathbf{s}_0, [\mathbf{s}_{\text{con},\ell}]_{\ell \in \mathcal{L}}]_{t \in \mathcal{T}}}}{\text{minimize}} & f(\cdot) \\ & \text{subject to} \\ & \text{Eqs. (10) and (11) Power flow linearization} \\ & \mathbf{W}_0[t] = \mathbf{v}_{\text{ref}}[t] \mathbf{v}_{\text{ref}}[t]^H \quad t \in \mathcal{T} \quad (12a) \\ & \text{diag}(\mathbf{W}_n[t])^\phi \geq (u_{\min,n}^\phi)^2 \quad \phi \in \Phi_n, n \in \mathcal{N}^+, t \in \mathcal{T} \quad (12b) \\ & \text{diag}(\mathbf{W}_n[t])^\phi \leq (u_{\max,n}^\phi)^2 \quad \phi \in \Phi_n, n \in \mathcal{N}^+, t \in \mathcal{T} \quad (12c) \\ & \text{Eq. (9c)} \quad \text{Transformer rating} \\ & \text{Eqs. (9d) to (9g)} \quad \text{Controllable loads} \\ & \quad \text{box constraints.} \end{aligned}$$

Equation (12a) sets the voltage in the reference bus while Eqs. (12b) and (12c) again enforce lower and upper bounds on voltage magnitudes. Although Eq. (9c) is non-linear, it remains convex and can be represented as a second-order cone. To obtain a linear program (LP), we approximate it with a linear inner space (i.e., a 12-face polygon) [43].

The BFM-LP Eq. (12) has $T(\sum_{n \in \mathcal{N}} |\Phi_n|^2 + 2 \sum_{(n,o) \in \mathcal{E}} |\Phi_{n,o}| + 2|\Phi_0| + 2 \sum_{\ell \in \mathcal{L}} |\Phi_{n_\ell}|)$ decision variables. Here, the dominant term $T \sum_{n \in \mathcal{N}} |\Phi_n|^2$ admits an upper bound $\mathcal{O}(T|\mathcal{N}|)$.

A few comments are in order. First, we use a linear power flow surrogate which entails the approximation of indirect variables. We discuss its validity and attenuate potential constraint violations in Section V. Second, by using the BFM-LP surrogate we treat link losses and voltage ratios as fixed parameters. Even by assuming zero link losses and perfectly balanced voltage ratios results show sufficient accuracy [26]. By using reasonable estimates of the fixed parameters, we further increase this accuracy [41]. Third, we used a linear inner space to approximate Eq. (9c) which is equivalent to conservatively approximating a circle with a regular polygon. This approximation is reasonable when the polygon has a sufficient number of faces. We use a 12-face polygon which covers more than 95% of the circle's area.

IV. INTERACTION BETWEEN AN ELECTRIC AMoD SYSTEM AND POWER DISTRIBUTION NETWORKS

In this section, we develop a model for the joint optimization of an electric AMoD system and the corresponding PDNs. As an electric AMoD system usually spans across multiple (disconnected) PDNs, we first introduce the multi-OPF problem which combines multiple OPF problem instances. Then, we formalize the coupling between the electric AMoD system and the PDNs before we state the joint AMoD-OPF problem.

A. Multi-OPF problem

The multi-OPF problem couples D instances of the OPF problem and results straightforwardly by extending the constraints for each instance $d \in \mathcal{D} = \{1, \dots, D\}$:

$$\begin{aligned} & \underset{\substack{[\mathbf{v}_n]_{n \in \mathcal{N}}, \mathbf{s}_0, \\ [\mathbf{s}_{\text{con},\ell}]_{\ell \in \mathcal{L}}]_{t \in \mathcal{T}, d \in \mathcal{D}}}}{\text{minimize}} & f(\cdot) \\ & \text{subject to} \\ & [\text{Eq. (6)}]_{d \in \mathcal{D}} \quad \text{Voltage at reference bus} \quad (13a) \\ & [\text{Eq. (7)}]_{d \in \mathcal{D}} \quad \text{Power injections} \quad (13b) \\ & [\text{Eq. (8)}]_{d \in \mathcal{D}} \quad \text{Power flow equation} \quad (13c) \\ & [\text{Eqs. (9a) and (9b)}]_{d \in \mathcal{D}} \quad \text{Bounds on voltage} \\ & \quad \text{magnitude} \quad (13d) \\ & [\text{Eq. (9c)}]_{d \in \mathcal{D}} \quad \text{Substation transformer} \\ & \quad \text{rating} \quad (13e) \\ & [\text{Eqs. (9d) to (9g)}]_{d \in \mathcal{D}} \quad \text{Controllable loads} \\ & \quad \text{box constraints} \quad (13f) \end{aligned}$$

Analogously to the single instance OPF problem, we derive a linear surrogate multi-OPF problem by replacing the power flow equation Eq. (8) with the BFM approximation Eqs. (10) and (11).

We neglect couplings upstream of PDN substations through the transmission network because this paper focuses solely on the interaction between an electric AMoD system and a series of PDNs. Couplings between the electric AMoD system and the power network at the transmission and distribution level occur on very different spatial scales (tens of kilometers vs. hundreds of meters), and result in largely orthogonal effects: specifically, couplings at the transmission level mainly influence bulk electricity prices [25], whereas couplings at the distribution level influence bus voltages and power losses. Accordingly, due to the orthogonal nature of the two couplings, we envision that a nested optimization approach could be used to first address transmission-level couplings through existing algorithms [e.g., 25], and then optimize distribution-level couplings through the tools proposed in this paper.

B. Coupling of the electric AMoD system and power distribution networks

Recall that charging stations, which appear as controllable loads in the PDNs, couple the electric AMoD system to the PDNs (see Fig. 1). Let $\mathcal{M}_{\mathcal{S}, \mathcal{A}_S} : \mathcal{S} \times \mathcal{T} \rightarrow \mathcal{A}_S$ be the function

mapping a charging station $s \in \mathcal{S}$ for each time step $t \in \mathcal{T}$ to all arcs in \mathcal{A}_S that represent charging vehicles at this station

$$\mathcal{M}_{\mathcal{S}, \mathcal{A}_S}(s, t) = \{(\mathbf{v}, \mathbf{w}) \in \mathcal{A}_S \mid v_{\mathbf{v}} = v_{\mathbf{w}} = s, c_{\mathbf{v}} < c_{\mathbf{w}}, t_{\mathbf{v}} \leq t \leq t_{\mathbf{w}}\}.$$

Then, the load at charging station s results to

$$p_s[t] = E_c \delta_{C,s} \sum_{(\mathbf{v}, \mathbf{w}) \in \mathcal{M}_{\mathcal{S}, \mathcal{A}_S}(s, t)} \sum_{m=0}^M f_m(\mathbf{v}, \mathbf{w}) \quad (14)$$

$$s \in \mathcal{S}, t \in \mathcal{T}$$

Each charging station $s \in \mathcal{S}$ relates to a controllable load in one of the PDNs through the mapping function $\mathcal{M}_{\mathcal{S}, \mathcal{L}} : \mathcal{S} \rightarrow (\mathcal{L} \times \mathcal{D})$. Formally, we attach charging station s to bus $n_{\mathcal{M}_{\mathcal{S}, \mathcal{L}}(s)}$ in PDN $d_{\mathcal{M}_{\mathcal{S}, \mathcal{L}}(s)}$. As we consider three-phase charging stations, we assume equally distributed loads,

$$s_{\text{con}, \mathcal{M}_{\mathcal{S}, \mathcal{L}}(s)}^a[t] = s_{\text{con}, \mathcal{M}_{\mathcal{S}, \mathcal{L}}(s)}^b[t] = s_{\text{con}, \mathcal{M}_{\mathcal{S}, \mathcal{L}}(s)}^c[t] = \frac{1}{3} p_s[t] \quad (15)$$

$$s \in \mathcal{S}, t \in \mathcal{T}.$$

Note that we can model four-quadrant inverters to control the load power factor [cf. 44] since $q_{\text{con}, \mathcal{M}_{\mathcal{S}, \mathcal{L}}(s)}^\phi$ must not necessarily be zero. Further, we can model balancing inverters [cf. 45] by changing the distribution of p_s among phases.

C. AMoD-OPF problem

Based on IV-A and IV-B, we state the joint AMoD-OPF problem:

$$\begin{aligned} & \underset{\substack{f_0, [\lambda_m^{c, \text{in}}]_{c \in \mathcal{C}}, \\ [\lambda_m^{t, c, \text{out}}]_{c \in \mathcal{C}, t \in \mathcal{T}, N_I, N_F}, \\ [\mathbf{v}_n]_{n \in \mathcal{N}}, [\mathbf{i}_{n, o}^\phi]_{(n, o) \in \mathcal{E}}, \\ \mathbf{s}_0, [\mathbf{s}_{\text{con}, t}]_{t \in \mathcal{T}, d \in \mathcal{D}}}}{\text{minimize}} & V_D \sum_{(\mathbf{v}, \mathbf{w}) \in \mathcal{A}} d_{v_{\mathbf{v}}, v_{\mathbf{w}}} f_0(\mathbf{v}, \mathbf{w}) \\ & + \sum_{t \in \mathcal{T}} \Delta t \sum_{d \in \mathcal{D}} V_{\text{el}, d}[t] \sum_{\phi \in \Phi} p_{0, d}^\phi[t] \end{aligned} \quad (16a)$$

subject to

Eqs. (1) to (4) and

Eqs. (5b) to (5e) Electric AMoD system

Eqs. (13a) to (13f) PDNs

Eqs. (14) and (15) Coupling from charging stations.

The objective Eq. (16a) comprises operating cost for both the electric AMoD fleet and the PDNs since we consider full cooperation between both operators. Analogously to the isolated electric AMoD problem Eq. (5a), we consider only rebalancing cost for the AMoD fleet. In each distribution network $d \in \mathcal{D}$, we account for the electricity cost that results from charging vehicles, uncontrollable loads, and power losses.

Note that our joint problem formulation treats both operators as a single entity, assuming complete information and cooperation. This assumption is in line with our mesoscopic view and scope to estimate an *upper bound* on the benefit of coordination and cooperation between both systems. We leave the study of game-theoretic aspects to future work where we intend to develop pricing and coordination mechanisms to align the incentives of the electric AMoD operator and

the PDN operators, and to leverage distributed optimization algorithms to compute a solution to the AMoD-OPF problem Eq. (16) in a distributed manner.

V. CASE STUDY IN ORANGE COUNTY, CA

We consider commuting trips within the cities of Fountain Valley, Irvine, North Tustin, Orange, Santa Ana, Tustin, and Villa Park, located in Orange County, CA with a total population of 834,901 [46]. In the following, we detail our data (V-A), before outlining the experimental design (V-B), and discussing our results (V-C)

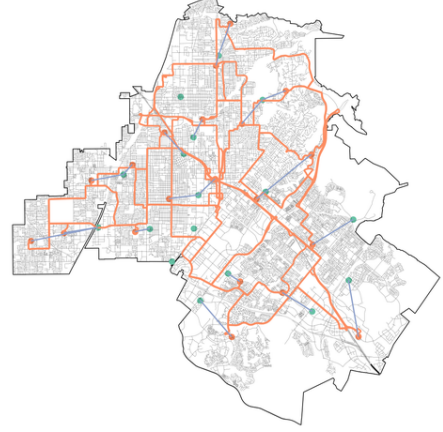


Fig. 3: Area considered in the Orange County, CA case study. The aggregated road network is shown in orange, representing vertices as dots and arcs as lines. Green dots show the substation locations. Blue lines show the assignment of a charging station to its closest substation.

A. Model parameters

We focus on an eight-hour commuting cycle from 5 am to 1 pm on July 3, 2015, discretized into six-minute steps, such that $|\mathcal{T}| = 80$. For this period, we model charging station networks and the transportation network at a mesoscopic aggregation level that allows a sufficient level of detail to analyze the interaction between an electric AMoD system and the PDNs, and ensures computational tractability.

a) *Transportation network data:* We derive trip demand from Census Tract Flow data from the 2006-2010 American Community Survey [47]. From these data, we take the estimated commuting flows between the 143 census tracts that are part of our case study. To align the granularity of aggregated charging station network representations and census tracts, we cluster the 143 census tracts into 20 larger areas using a k-means algorithm. We neglect commuting flows if they start or end outside the area of our case study or if they start and end within the same cluster. We use the mobility demand over time distribution of McKenzie and Rapino [48] to proportionally sample the time-independent census tract flows to our planning horizon, such that our planning horizon comprises 122,219 trips (32.8%) out of a total of 372,656 daily trips.

The problem of fleet sizing for (electric) AMoD systems [49], [50] exceeds the scope of this paper. For the purpose of this case study, we heuristically selected a fleet size that is large enough for the AMoD-OPF problem Eq. (16) to remain feasible but with only a small number of idle vehicles. This was done as follows: since the passenger-carrying trips are pre-routed and we require all trips to be serviced, the maximum number of concurrent passenger-carrying trips sets a lower bound on the number of required vehicles. The AMoD-OPF problem Eq. (16) will not be feasible if there are fewer vehicles than this. In fact, there must be more vehicles since some of them have to charge or do rebalancing at the time of peak concurrent passenger-carrying trips. For our parameters, the peak number of concurrent passenger-carrying trips was 11,237 at 7:30 am (see Fig. 6). We started by setting the fleet size to two times this number and then decreasing it by 0.1 until the problem was no longer feasible. This occurred at 1.3. Hence, we chose 1.4 times the peak number concurrent of passenger-carrying trips as fleet size which results, due to rounding, in 15,732 vehicles.

On the same granularity level, we create an aggregated road network based on OpenStreetMap data [51], [52]. We choose the road network vertices closest to the centroids of the census tract clusters and add arcs between these vertices if a connection exists in the real road network. Doing so, we obtain an aggregated road network with 20 vertices and 76 arcs (see Fig. 3).

For each aggregated road network vertex, we consider three-phase 50-kilowatt DC fast charging stations with $\bar{S}_s = 40$ plugs in total. Accordingly, each vertex has a charging station with a maximum load of two megawatts (0.66 megawatts per phase).

b) Electric vehicle data: We consider a homogeneous vehicle fleet based on the characteristics of the Nissan Leaf 2018 [53] which has a 40-kilowatt hour battery and a range of 243 kilometers. Based on fast-charging guidelines, we reduce a vehicle's battery capacity and its range to 80 percent of their original values [15]; and discretize this effective battery capacity into $C = 40$ steps. To account for the possibility that vehicles might not start the day with fully charged batteries, we set the SoC at $t = 1$ to 50%. Furthermore, we require vehicles to recharge the amount of energy used over a planning horizon such that the final SoC must be at minimum 50% again. We set the vehicle operation cost per unit distance (excluding electricity) to $V_D = 0.3 \text{ USD/km}$ [54].

c) Power distribution networks data: As a proxy for (sub-)urban distribution networks, we use a GridLAB-D model of the PL-1 distribution network, a primary feeder in California, USA operated by the Pacific Gas and Electric Company (PG&E) which is publicly available for research purposes [55]. The network comprises 322 buses and operates at a nominal voltage of 12.6 kilovolts. We set the uncontrollable loads to the model's time-varying loads.

We take the location of substations from the utility's data [56] and attach a model of the PL-1 distribution network to each substation. We set the electricity price at each substation to the corresponding locational marginal price [57] and conservatively assume a base load utilization of 75 percent at

the substation transformer. Typically, distribution networks are operated at 50 to 75 percent of their load capacity so that loads can be transferred from one distribution network to another if needed [58]. Accordingly, we set the substation transformer rating \hat{s}_0 to $1/0.75$ times the value of the peak base load (i.e., without charging stations), yielding $\hat{s}_0 = 10.42 \text{ MVA}$. In addition, we set the lower voltage magnitude limit to 0.96 per-unit and the upper limit to 1.04 per-unit, which is 0.01 per-unit tighter than required by ANSI C84.1 to allow for the voltage drop in the secondaries of the network.

We connect each charging station to the distribution network whose substation is nearest. Since no data on the coordinates of the distribution network buses exist, we randomly attach the charging station to one of the PDN buses. Accordingly, the PDN is the same for each substation, except for the varying number and location of charging stations. In total, we consider 14 distribution networks, each with one or two charging stations.

We determine the price of electricity $V_{el,s}$ at a certain charging station to be equal to the electricity price at the respective substation, such that $V_{el,s}[t] = V_{el,d_{MS,L(s)}}[t]$ holds. Given that we focus on the total benefit from a system perspective and treat both operators as a single entity, only the spatial variation of electricity prices which is closely linked to the substation prices affects our solution.

Some comments on the distribution network modeling are in order: first, we used the same network model and load values for each distribution network, considering loads from a single summer day. As PDNs are treated as critical infrastructure and load data is usually confidential to protect customers, more accurate data is not publicly available for research purposes [59]. However, our model can be rerun with more accurate data at any time. Second, we set the electricity price at each substation to the corresponding locational marginal price. Locational marginal prices result from the power consumption at the transmission grid level. As our focus is on the interaction of the electric AMoD fleet with the distribution grids and the power used for recharging represents only a negligible fraction at transmission grid level, neglecting the impact of this consumption on the marginal prices does not affect the accuracy of our results. Third, we assume the electricity price for charging at a certain station to be equal to the electricity price at the respective substation. This is consistent with our system perspective where only the spatial variation of electricity prices is relevant.

The resulting AMoD-OPF problem has 6,224,240 decision variables. From these, 1,463,600 come from the electric AMoD part of the problem and 4,760,640 come from the multi-OPF part. Given that we are using the same distribution network model, the number of variables in the multi-OPF part admits the upper bound $\mathcal{O}(TD|\mathcal{N}|)$. Thus, we have the following upper bound for the number of decision variables in the whole AMoD-OPF problem: $\mathcal{O}(T(C|\mathcal{V}_R|^2 + D|\mathcal{N}|))$.

Nominally, the size of the electric AMoD part of the problem increases quadratically with the number of road vertices. However, if more vertices are added for the same area, the road segment arcs will become shorter. In this case, T and C should be increased to capture the reduced travel duration and

energy consumption in the shorter road segment arcs. Thus, in practice, the electric AMoD part of the problem grows more than quadratically with the number of road vertices. This feature of the AMoD-OPF problem limits our formulation to rather coarse road networks.

B. Experimental design

To quantify the impact of an electric AMoD system on the PDNs and the benefit of optimized joint coordination, our experiments consider two cases: first, we analyze the impact of an electric AMoD system on the PDNs without coordination, i.e., the uncoordinated case. These results show how electric AMoD systems (negatively) affect PDNs. Then, we focus on the coordinated case in which the electric AMoD system and the distribution networks are jointly optimized. Comparing the results of both cases allows quantifying the potential of optimized coordination between these systems. In both cases we generate results as follows:

- 1) Computing controllable loads: we determine the load at each charging station that result from the operation of the electric AMoD system. Depending on the studied case, we solve either Eq. (5) or Eq. (16). By doing so, we determine the controllable loads in both cases.
- 2) Solving the power flow equation: to assess the quality of a solution from step 1, we solve the exact power flow equation Eq. (8) to derive the true values of the indirect variables (i.e., complex power injection at the reference bus and complex voltage in all other buses).
- 3) Evaluating constraint violations: we determined controllable loads without an exact model of the PDNs as it was either neglected (uncoordinated case) or approximated (coordinated case). Hence, it is most likely that the solutions entail certain constraint violations. To quantify these violations, we evaluate integral constraint violations as we consider a time-variant model. In practice, regulations require voltage magnitudes to be kept within a given percentage of a nominal value (e.g., ANSI C84.1). Hence, we analyze the integral voltage magnitude constraint violation

$$u_{\text{viol}} = \sum_{t \in \mathcal{T}} \Delta t \sum_{d \in \mathcal{D}} \sum_{n \in \mathcal{N}_d^+} \sum_{\phi \in \Phi_{n,d}} \left((u_{\min,n,d}^\phi - u_{n,d}^\phi[t])^+ + (u_{n,d}^\phi[t] - u_{\max,n,d}^\phi)^+ \right)$$

with $(x)^+ = \max(x, 0)$, $x \in \mathbb{R}$.

Substations typically connect distribution networks to the higher-voltage transmission network, requiring a transformer to lower the voltage. In order to avoid overloading this transformer, the power draw must be less than the transformer rating. Hence, we analyze the integral substation transformer rating violation

$$\hat{s}_{0,\text{viol}} = \sum_{t \in \mathcal{T}} \Delta t \sum_{d \in \mathcal{D}} \left(\sum_{\phi \in \Phi_{0,d}} s_{0,d}^\phi[t] - \hat{s}_{0,d} \right)^+.$$

- 4) Evaluating energy consumption and cost: we analyze the energy consumption of the electric AMoD system and

its cost. For this purpose, we separate the total energy consumption $E_{\text{total}} \in \mathbb{R}$ into two components:

$$E_{\text{total}} = E_{\text{total,base}} + E_{\text{AMoD}}, \quad (17)$$

where $E_{\text{total,base}} \in \mathbb{R}$ is the total energy consumption in the base case (i.e., without the electric AMoD system) and $E_{\text{AMoD}} \in \mathbb{R}$ is the additional energy consumption caused by the electric AMoD system.

The total energy consumption results from summing the energy draw of all substations

$$E_{\text{total}} = \sum_{t \in \mathcal{T}} \Delta t \sum_{d \in \mathcal{D}} \sum_{\phi \in \Phi_{0,d}} p_{0,d}^\phi[t].$$

It includes the energy consumed by exogenous loads and the electric AMoD system.

The total energy consumption in the base case results analogously without considering an electric AMoD system

$$E_{\text{total,base}} = \sum_{t \in \mathcal{T}} \Delta t \sum_{d \in \mathcal{D}} \sum_{\phi \in \Phi_{0,d}} p_{\text{base},d}^\phi[t].$$

Here, $p_{\text{base},d}^\phi \in \mathbb{R}$ is the power drawn in phase $\phi \in \Phi_0$ from substation $d \in \mathcal{D}$.

It follows from Eq. (17) that the difference of E_{total} and $E_{\text{total,base}}$ represents the additional energy consumption caused by the electric AMoD system:

$$E_{\text{AMoD}} = E_{\text{total}} - E_{\text{total,base}}.$$

The electric AMoD operator would have to pay for this energy. Its cost is given by

$$V_{\text{el,AMoD}} = \sum_{t \in \mathcal{T}} \Delta t \sum_{d \in \mathcal{D}} V_{\text{el},d}[t] \sum_{\phi \in \Phi_{0,d}} (p_{0,d}^\phi[t] - p_{\text{base},d}^\phi[t]).$$

Due to losses in the distribution networks, not all of E_{AMoD} relate to charging stations. The energy delivered to the charging stations is given by

$$E_{\text{charge,AMoD}} = \sum_{t \in \mathcal{T}} \Delta t \sum_{d \in \mathcal{D}} \sum_{\ell \in \mathcal{L}_d} \sum_{\phi \in \Phi_{n_\ell,d}} p_{\text{con},\ell,d}^\phi[t].$$

The difference between E_{AMoD} and $E_{\text{charge,AMoD}}$ represents the link losses caused by the electric AMoD system:

$$E_{\text{loss,AMoD}} = E_{\text{AMoD}} - E_{\text{charge,AMoD}}.$$

Analogously, the cost of these losses is given by

$$V_{\text{el,loss,AMoD}} = V_{\text{el,AMoD}} - V_{\text{el,charge,AMoD}}$$

where $V_{\text{el,charge,AMoD}}$ is the cost of $E_{\text{charge,AMoD}}$:

$$V_{\text{el,charge,AMoD}} = \sum_{t \in \mathcal{T}} \Delta t \sum_{d \in \mathcal{D}} V_{\text{el},d}[t] \sum_{\ell \in \mathcal{L}_d} \sum_{\phi \in \Phi_{n_\ell,d}} p_{\text{con},\ell,d}^\phi[t].$$

Our implementation builds on top of the AMoD Toolkit¹ which relies on YALMIP [60] to formulate and solve electric AMoD problems. Additionally, we built a general codebase

¹<https://github.com/StanfordASL/AMoD-toolkit>

for unbalanced OPF problems, the Unbalanced OPF Toolkit². To support future research in this field, we released both the AMoD Toolkit and the Unbalanced OPF Toolkit under an open license. We used Gurobi [61] to solve the resulting optimization problems.

C. Results and discussion

Following our experimental design, we evaluate constraint violations (Figs. 4 and 5), as well as energy consumption and costs (Table I).

Figure 4 shows a box plot with voltage levels for all buses and time steps in all distribution networks, including corresponding limits for the coordinated, the uncoordinated and the base case without the electric AMoD system. The base case shows no violations while violations appear in both cases where the electric AMoD system is included. As can be seen, optimized coordination between the electric AMoD system and the PDNs helped to decrease the number and extent of voltage constraint violations significantly. Especially when large violations arise in the uncoordinated case, optimized coordination offers a significant improvement potential. Coordination between both systems reduced integral voltage magnitude constraint violation by 50.28 percent, from 24.04 per-unit hour to 11.95 per-unit hour. Consequently, coordination between both systems helps to achieve better compliance with regulations that require the voltage magnitude to be kept close to its nominal value, e.g., ANSI C84.1.

Figure 5 shows the transformer capacity violations for two distribution networks that differ in the number of connected charging stations. While the Bryan network covers two charging stations, the Irvine network covers only one charging station. The plot shows the substation load, separated in its base load and additional load caused by recharging, as well as the price for electricity at the substation as a function of time for both the coordinated and the uncoordinated case. As can be seen, the additional load in Bryan is higher than in Irvine. This is caused by the number of connected charging stations, as each charging station can cause at maximum an additional load of two megawatts. Consequently, in the uncoordinated case, a substation capacity constraint violation arises for Bryan, while Irvine remains feasible over the whole time horizon.

As can be seen, coordination helps to resolve the substation capacity constraint violation for Bryan, as charging loads that exceed the capacity constraint are shifted to later time steps. However, this implies higher electricity prices for recharging. Even though the substation capacity constraint is not active in the uncoordinated case for Irvine, we see a decreased substation load in the coordinated case. This decrease results from fewer vehicles charging in Irvine due to its large voltage magnitude violations in the uncoordinated case. Here, resolving the voltage magnitude violation directly correlates with a decreased substation load.

The results of Bryan and Irvine are indicative of those of the other 12 distribution networks. All in all, optimized coordination nearly eliminated substation capacity constraint

violations, reducing them by 99.71, from 7.89 mega volt-ampere hour to 0.02 mega volt-ampere hour.

Concluding, optimized coordination helps to reduce substation loads and related capacity constraint violations and thus diminishes the risk of brown-outs due to overloaded substations and prolongs transformer life.

Table I shows the impact of coordinating an electric AMoD fleet with PDNs under a system optimal objective. As can be seen, the total operational costs of the electric AMoD system increase slightly by 3.13 percent (3,329.61 USD). Rebalancing costs show an increase of 3.28 percent (3,206.47 USD) as vehicles charging in more distant charging stations due to coordination increase rebalancing detours. Coherently, the total consumed electricity also increases in the coordinated case. As coordination partly shifts vehicles' charging activities to time steps with higher electricity prices (see Fig. 5), electricity costs also increase by 1.42 percent (123.15 USD). Figure 6 further verifies this effect, as it shows a steady charging activity after 11 am for the coordinated case, whereas charging activities decrease significantly after 11 am in the uncoordinated case. The small increase in operational costs is the price we pay for reducing system constraint violations. In exchange, we get improved voltage profiles and prolonged transformer life.

The energy delivered to the charging stations (see Table I) increases by 1.82 megawatt hours (0.68 percent) in the coordinated case because of increased rebalancing detours. However, the energy attributable to the electric AMoD system consumed at the substations increases only by 1.24 megawatt hour (0.44 percent). The difference of 0.58 megawatt hour is due to energy losses being reduced by 5.24 percent. Fewer energy losses reflect more efficient power distribution: a greater share of the energy leaving the substations reaches the charging stations in the coordinated case (96.29 percent compared with 96.07 percent).

The AMoD-OPF problem Eq. (16) was solved in 0.7 hours, whereas solving the electric AMoD problem Eq. (5) took 8.1 hours. Accordingly, the presented solution approach is not suitable to be extended to a receding-horizon based real-time control framework. However, the results of these studies can be used to identify bottlenecks in PDNs which point at necessary grid extension investments. Further, a grid operator can use this approach to compute the amount of spinning reserves needed to hedge on the day-ahead market to secure a stable operation of its PDNs.

VI. CONCLUSION

We presented the AMoD-OPF problem that combines an electric AMoD problem with a multi-OPF problem. In this context, we discussed power flow surrogates to obtain a computationally tractable convex problem formulation. The resulting AMoD-OPF problem allows to determine an *upper bound* on the benefit of coordinating an electric AMoD system and a series of PDNs. With this methodological framework, we investigated the impact of an electric AMoD system on the PDNs. Herein, we especially focused on the benefits of coordination between both systems and discussed results for a case study in Orange County, CA. We showed that in an uncoordinated system, the electric AMoD fleet negatively affects

²<https://github.com/StanfordASL/unbalanced-opf-toolkit>

	Uncoord	Coord	Change [%]
Electricity cost, charging	8.35	8.49	1.67
Electricity cost, losses	0.35	0.33	-4.59
Electricity cost, AMoD	8.69	8.82	1.42
Rebalancing cost	97.79	101.00	3.28
Total cost, AMoD	106.49	109.82	3.13
Energy, charging	268.82	270.63	0.68
Energy, losses	11.01	10.43	-5.24
Energy, AMoD	279.82	281.06	0.44

TABLE I: Cost in thousands of USD (kUSD) and energy consumption in MWh of operating the electric AMoD system.

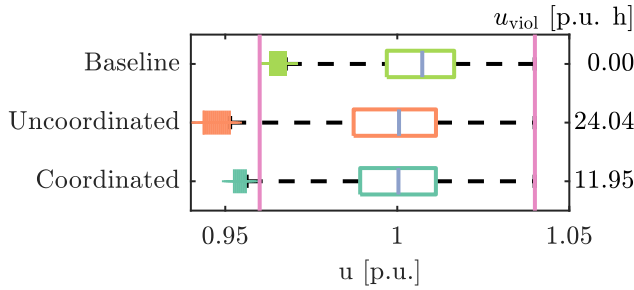


Fig. 4: Violation of voltage magnitude constraint. The plot shows voltage magnitudes for the baseline, the uncoordinated, and the coordinated case. Voltage magnitude bounds are shown with pink lines. The integral constraint violation is shown on the right in per-unit hour. As can be seen, constraint violations only appear when the electric AMoD system is present. Then, the number and extent of constraint violations are significantly lower in the coordinated case.

the distribution networks: the charging behavior of the electric AMoD vehicles caused overloads at substation transformers and violated (lower) voltage magnitude limits. Furthermore, we showed that a coordinated system helps to balance the load in the PDNs in time and space. Specifically, link losses were slightly reduced, substation overloads were nearly eliminated, and voltage violations were halved. Nonetheless, these reductions in constraint violations increased the cost of operating the electric AMoD system by 3.13 percent. This indicates that distribution networks can support more electric vehicles before upgrades are needed if the vehicles are charged in coordination with exogenous loads in the PDNs. Due to our system optimal objective, these findings remain as an upper bound to the overall benefit of coordination between an electric AMoD fleet and PDNs.

Our findings open the field for multiple directions of future research. First, our AMoD-OPF problem remains mesoscopic and thus, assumes perfect knowledge of future loads and trip requests. To design a real-time algorithm, the integration of forecasts to capture the stochastic nature of the problem depicts an interesting avenue for further research. Second, we modeled the operators of the AMoD fleet and the PDNs

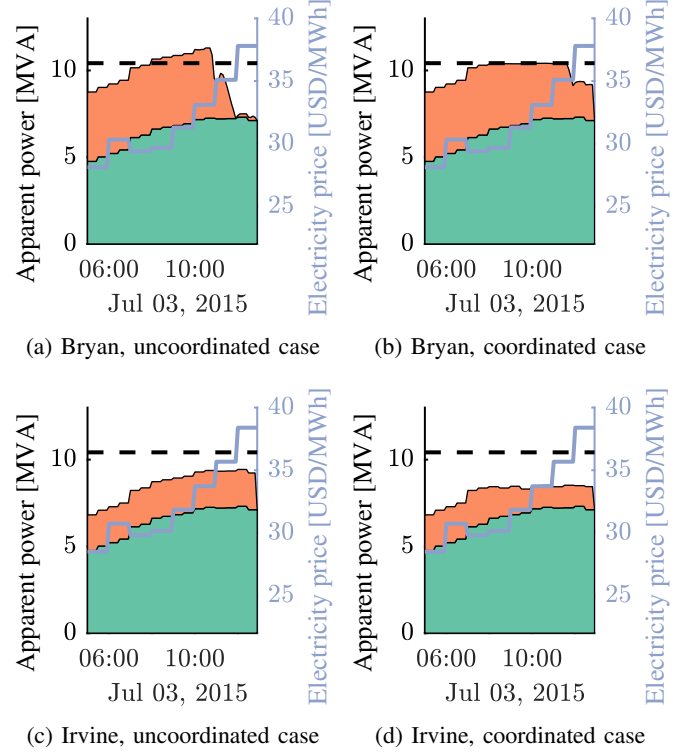


Fig. 5: Violation of substation capacity constraint. Legend: the green area depicts the base load, while the orange one shows additional load due to the electric AMoD system, and the dashed line is the substation transformer rating. In the uncoordinated case, the constraint is violated in Bryan. In the coordinated case, charging vehicles later during the day resolves the violation.

as a single entity, implying full cooperation. In future work, one should address the interplay between these two stakeholders and may aim at designing cooperative mechanisms or pricing policies to investigate market dynamics, e.g., the price of stability and the price of anarchy. Third, our case study remains as a first example that shows the benefit of coordinating electric AMoD fleets with PDNs. To provide profound decision support to practitioners one should analyze additional case studies that capture different PDNs, different road network characteristics, varying instance sizes, and distributed renewable energy generation. Fourth, our case study did not consider the EVs potential to feed power back into the PDN. Hence, extending our modeling approach for vehicle-to-grid options, evaluating regulation and operating reserve potentials, remains a promising avenue for future research.

ACKNOWLEDGMENTS

The authors thank Saverio Bolognani, David Chassin and Raffi Sevlian for sharing their insights on power systems.

REFERENCES

- [1] G. S. Bauer, J. B. Greenblatt, and B. F. Gerke, "Cost, energy, and environmental impact of automated electric taxi fleets in manhattan," *Environmental Science & Technology*, vol. 52, no. 8, pp. 4920–4928, 2018.

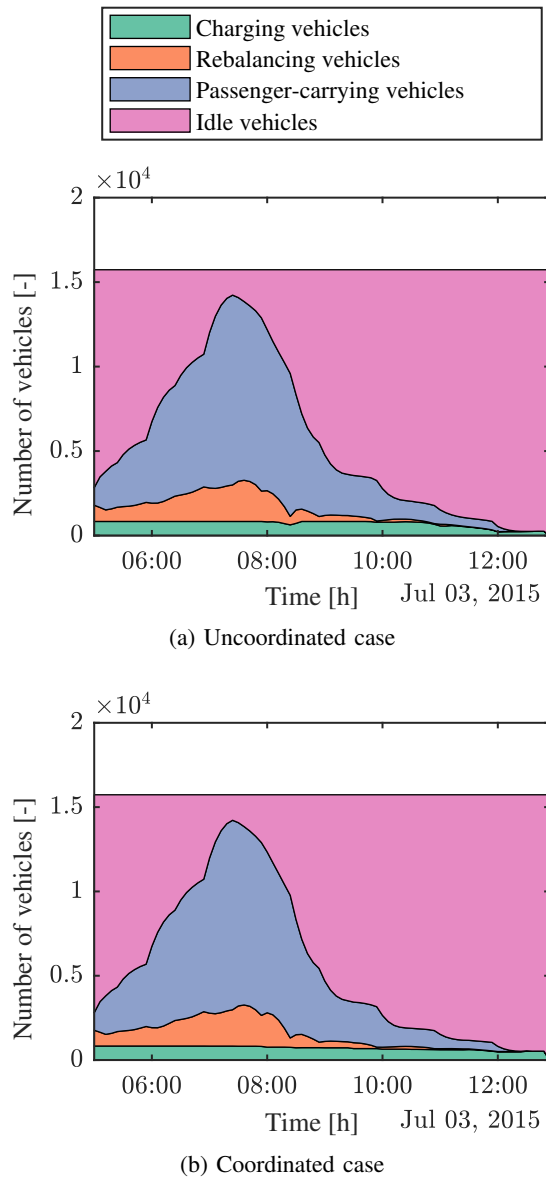


Fig. 6: Fleet activity during the day: more vehicles charge after 11:30 in the coordinated case than in the uncoordinated one. At this time, the electricity price is higher but the network has spare capacity such that coordination shifts charging to reduce constraint violations.

- [2] K. Spieser, K. Treleaven, R. Zhang, E. Frazzoli, D. Morton, and M. Pavone, "Toward a systematic approach to the design and evaluation of Autonomous Mobility-on-Demand systems: A case study in Singapore," in *Road Vehicle Automation*, Springer, 2014.
- [3] E. Hannon, C. McKerracher, I. Orlandi, and S. Ramkumar, "An integrated perspective on the future of mobility," McKinsey & Company, Tech. Rep., 2016, Available at <https://www.mckinsey.com/business-functions/sustainability-and-resource-productivity/our-insights/an-integrated-perspective-on-the-future-of-mobility>.
- [4] P. M. Boesch, F. Becker, H. Becker, and K. W. Axhausen, "Cost-based analysis of autonomous mobility services," *Transport Policy*, vol. 64, pp. 76–91, 2018.
- [5] H. Shareef, M. M. Islam, and A. Mohamed, "A review of the stage-of-the-art charging technologies, placement methodologies, and impacts of electric vehicles," *Renewable and Sustainable Energy Reviews*, vol. 64, pp. 403–420, 2016.
- [6] P. Richardson, D. Flynn, and A. Keane, "Optimal charging of electric vehicles in low-voltage distribution systems," *IEEE Transactions on Power Systems*, vol. 27, no. 1, pp. 268–279, 2012.
- [7] K. Clement-Nyns, E. Haesen, and J. Driesen, "The impact of charging plug-in hybrid electric vehicles on a residential distribution grid," *IEEE Transactions on Power Systems*, vol. 25, no. 1, pp. 371–380, 2010.
- [8] M. Pavone, S. L. Smith, E. Frazzoli, and D. Rus, "Robotic load balancing for Mobility-on-Demand systems," *Int. Journal of Robotics Research*, vol. 31, no. 7, pp. 839–854, 2012.
- [9] J. Bischoff and M. Maciejewski, "Simulation of city-wide replacement of private cars with autonomous taxis in berlin," *Procedia Computer Science*, vol. 83, pp. 237–244, 2016.
- [10] D. J. Fagnant and K. M. Kockelman, "The travel and environmental implications of shared autonomous vehicles, using agent-based model scenarios," *Transportation Research Part C: Emerging Technologies*, vol. 40, pp. 1–13, 2014.
- [11] F. Rossi, R. Zhang, Y. Hindy, and M. Pavone, "Routing autonomous vehicles in congested transportation networks: Structural properties and coordination algorithms," *Autonomous Robots*, vol. 42, no. 7, pp. 1427–1442, 2018.
- [12] M. Salazar, F. Rossi, M. Schiffer, C. H. Onder, and M. Pavone, "On the interaction between autonomous mobility-on-demand and the public transportation systems," in *PROC. IEEE INT. CONF. ON INTELLIGENT TRANSPORTATION SYSTEMS*, In Press. Extended Version, Available at <https://arxiv.org/abs/1804.11278>, 2018.
- [13] R. Zhang and M. Pavone, "Control of robotic Mobility-on-Demand systems: A queueing-theoretical perspective," *Int. Journal of Robotics Research*, vol. 35, no. 1–3, pp. 186–203, 2016.
- [14] M. Volkov, J. Aslam, and D. Rus, "Markov-based redistribution policy model for future urban mobility networks," in *PROC. IEEE INT. CONF. ON INTELLIGENT TRANSPORTATION SYSTEMS*, 2012.
- [15] D. T. Chen, K. M. Kockelman, and J. P. Hanna, "Operations of a shared, autonomous, electric vehicle fleet: Implications of vehicle & charging infrastructure decisions," *Transportation Research Part A: Policy and Practice*, vol. 94, pp. 243–254, 2016.
- [16] J. Munkhammar and M. Shepero, "Autonomous electric vehicle fleet charging in cities: Optimal utility estimates and monte carlo simulations," in *IEEE PES INNOVATIVE SMART GRID TECHNOLOGIES CONF. EUROPE*, 2017.
- [17] R. Zhang, F. Rossi, and M. Pavone, "Model predictive control of Autonomous Mobility-on-Demand systems," in *PROC. IEEE CONF. ON ROBOTICS AND AUTOMATION*, 2016.
- [18] F. Dandl and K. Bogenberger, "Comparing future autonomous electric taxis with an existing free-floating carsharing system," *IEEE Transactions on Intelligent Transportation Systems*, 2018.
- [19] R. Iglesias, F. Rossi, R. Zhang, and M. Pavone, "A BCMP network approach to modeling and controlling autonomous mobility-on-demand systems," *Int. Journal of Robotics Research*, 2018, In Press.
- [20] S. W. Hadley and A. A. Tsvetkova, "Potential impacts of plug-in hybrid electric vehicles on regional power generation," *The Electricity Journal*, vol. 22, no. 10, pp. 56–68, 2009.
- [21] M. Tran, D. Banister, J. D. K. Bishop, and M. D. McCulloch, "Realizing the electric-vehicle revolution," *Nature Climate Change*, vol. 2, no. 5, pp. 328–333, 2012.
- [22] M. Alizadeh, H.-T. Wai, M. Chowdhury, A. Goldsmith, A. Scaglione, and T. Javidi, "Optimal pricing to manage electric vehicles in coupled power and transportation networks," *IEEE Transactions on Control of Network Systems*, vol. 4, no. 4, pp. 863–875, 2017.

- [23] J. J. Q. Yu and A. Y. S. Lam, "Autonomous vehicle logistic system: Joint routing and charging strategy," *IEEE Transactions on Intelligent Transportation Systems*, vol. 19, no. 7, pp. 2175–2187, 2018.
- [24] R. Iacobucci, B. McLellan, and T. Tezuka, "Modeling shared autonomous electric vehicles: Potential for transport and power grid integration," *Energy*, vol. 158, pp. 148–163, 2018.
- [25] F. Rossi, R. Iglesias, M. Alizadeh, and M. Pavone, "On the interaction between Autonomous Mobility-on-Demand systems and the power network: Models and coordination algorithms," in *ROBOTICS: SCIENCE AND SYSTEMS*, Extended version available at <https://arxiv.org/abs/1709.04906>, 2018.
- [26] L. Gan and S. H. Low, "Convex relaxations and linear approximation for optimal power flow in multiphase radial networks," in *POWER SYSTEMS COMPUTATION CONFERENCE*, 2014.
- [27] W. H. Kersting, *Distribution system modelling and analysis*, First. CRC Press, 2002.
- [28] J. de Hoog, T. Alpcan, M. Brazil, D. A. Thomas, and I. Mareels, "Optimal charging of electric vehicles taking distribution network constraints into account," *IEEE Transactions on Power Systems*, vol. 30, no. 1, pp. 365–375, 2015.
- [29] R. Iacobucci, B. McLellan, and T. Tezuka, "Optimization of shared autonomous electric vehicles operations with charge scheduling and vehicle-to-grid," *Transportation Research Part C: Emerging Technologies*, vol. 100, pp. 34–52, 2019.
- [30] R. Iglesias, F. Rossi, K. Wang, D. Hallac, J. Leskovec, and M. Pavone, "Data-driven model predictive control of autonomous mobility-on-demand systems," in *PROC. IEEE CONF. ON ROBOTICS AND AUTOMATION*, 2018.
- [31] J. Glover, M. Sarma, and T. Overbye, *Power system analysis and design*, Fifth. Cengage Learning, 2011.
- [32] A. Bernstein and E. Dall'Anese, "Linear power-flow models in multiphase distribution networks," in *IEEE PES INNOVATIVE SMART GRID TECHNOLOGIES CONF. EUROPE*, 2017.
- [33] C. Zhao, E. Dall'Anese, and S. H. Low, "Optimal power flow in multiphase radial networks with delta connections," in *IREP BULK POWER SYSTEMS DYNAMICS AND CONTROL SYMPOSIUM*, 2017.
- [34] S. Sojoudi and S. H. Low, "Optimal charging of plug-in hybrid electric vehicles in smart grids," in *IEEE POWER AND ENERGY SOCIETY GENERAL MEETING*, 2011.
- [35] L. Hernandez, C. Baladron, J. M. Aguiar, B. Carro, A. J. Sanchez-Esguevillas, J. Lloret, and J. Massana, "A survey on electric power demand forecasting: Future trends in smart grids, microgrids and smart buildings," *IEEE Communications Surveys Tutorials*, vol. 16, no. 3, pp. 1460–1495, 2014.
- [36] J. A. Taylor, *Convex optimization of power systems*, First. Cambridge Univ. Press, 2015.
- [37] J. Lavaei and S. H. Low, "Zero duality gap in optimal power flow problem," *IEEE Transactions on Power Systems*, vol. 27, no. 1, pp. 92–107, 2012.
- [38] D. K. Molzahn and I. A. Hiskens, *A survey of relaxations and approximations of the power flow equations*, 1st ed. Now Foundations and Trends, 2019.
- [39] C. Coffrin, D. Gordon, and P. Scott. (2014). Nesta, the nicta energy system test case archive. Available at <http://arxiv.org/abs/1411.0359>.
- [40] A. Estandia, "On the interaction between autonomous mobility on demand systems and power distribution networks – an optimal power flow approach," Available at <https://www.research-collection.ethz.ch/handle/20.500.11850/340087>, Master's thesis, ETH Zurich, 2018.
- [41] M. D. Sankur, R. Dobbe, E. Stewart, D. S. Callaway, and D. B. Arnold. (2016). A linearized power flow model for optimization in unbalanced distribution systems. Available at <http://arxiv.org/abs/1606.04492>.
- [42] S. Bolognani and F. Dörfler, "Fast power system analysis via implicit linearization of the power flow manifold," in *ALLERTON CONF. ON COMMUNICATIONS, CONTROL AND COMPUTING*, 2015.
- [43] A. Barnes, H. Nagarajan, E. Yamangil, R. Bent, and S. Backhaus. (2017). Tools for improving resilience of electric distribution systems with networked microgrids. Available at <https://arxiv.org/abs/1705.08229>.
- [44] M. Kesler, M. C. Kisacikoglu, and L. M. Tolbert, "Vehicle-to-grid reactive power operation using plug-in electric vehicle bidirectional offboard charger," *IEEE Transactions on Industrial Electronics*, vol. 61, no. 12, pp. 6778–6784, 2014.
- [45] S. Weckx and J. Driesen, "Load balancing with ev chargers and pv inverters in unbalanced distribution grids," *IEEE Transactions on Sustainable Energy*, vol. 6, no. 2, pp. 635–643, 2015.
- [46] United States Census Bureau. (2010). Population, housing units, area, and density: 2010 - state - place and (in selected states) county subdivision 2010 census summary file 1. Available at https://factfinder.census.gov/bkmk/table/1.0/en/DEC/10_SF1/GCTPH1.ST10/0400000US34.
- [47] Federal Highway Administration, "Census Transportation Planning Products (CTTP) 2006-2010 Census Tract Flows," U.S. Dept. of Transportation, Tech. Rep., 2014. [Online]. Available: https://www.fhwa.dot.gov/planning/census%5C_issues/ctpp/data%5C_products/2006-2010%5C_tract%5C_flows/.
- [48] B. McKenzie and M. Rapino. (2011). Commuting in the united states: 2009. Available at <https://www2.census.gov/library/publications/2011/acs/acs-15.pdf>.
- [49] M. M. Vazifeh, P. Santi, G. Resta, S. H. Strogatz, and C. Ratti, "Addressing the minimum fleet problem in on-demand urban mobility," *Nature*, vol. 557, pp. 534–538, 2018.
- [50] H. Zhang, C. J. R. Sheppard, T. E. Lipman, and S. J. Moura. (2018). Joint fleet sizing and charging system planning for autonomous electric vehicles. Available at <https://arxiv.org/abs/1811.00234>.
- [51] M. Haklay and P. Weber, "OpenStreetMap: User-generated street maps," *IEEE Pervasive Computing*, vol. 7, no. 4, pp. 12–18, 2008.
- [52] G. Boeing, "OSMnx: New methods for acquiring, constructing, analyzing, and visualizing complex street networks," *Computers, Environment and Urban Systems*, vol. 65, pp. 126–139, Sep. 2017.
- [53] Nissan UK. (). 2018 nissan leaf. Available at <https://www.nissan.co.uk/vehicles/new-vehicles/leaf/range-charging.html>.
- [54] Bureau of Transportation Statistics, "National transportation statistics," U.S. Dept. of Transportation, Tech. Rep., 2016.
- [55] Pacific Gas and Electric Company. (). Pge_models. Available at https://sourceforge.net/p/gridlab-d/code/HEAD/tree/Taxonomy_Feeder/PGE_Models/.
- [56] Southern California Edison. (). Substations. Available at http://data-sce2.opendata.arcgis.com/datasets/_0.
- [57] California Independent System Operator. (). Locational marginal prices (lmp). Available at <http://oasis.caiso.com/mrioasis/logon.do>.
- [58] K. P. Schneider, Y. Chen, D. P. Chassin, R. Pratt, D. Engel, and S. Thompson, "Modern grid initiative distribution taxonomy final report," Tech. Rep., 2008, Available at https://www.pnnl.gov/main/publications/external/technical_reports/PNNL-18035.pdf.
- [59] F. E. P. Marcos, C. M. Domingo, T. G. S. Roman, B. Palmintier, B.-M. Hodge, V. Krishnan, F. de Cuadra Garcia, and B. Mather, "A review of power distribution test feeders in the united states and the need for synthetic representative networks," *Energies*, vol. 10, no. 11, 2017.
- [60] J. Löfberg, "YALMIP : A toolbox for modeling and optimization in MATLAB," in *IEEE INT. SYMP. ON COMPUTER AIDED CONTROL SYSTEMS DESIGN*, 2004.
- [61] Gurobi Optimization, LLC, *Gurobi optimizer reference manual*, Available at <http://www.gurobi.com>, 2018.